

Supplementary Tables

Table S1: Average Fe fractions (%), for the years 2000-2014, applied in the model on dust minerals, as well as on the anthropogenic combustion and the biomass burning sectors, to represent the emitted Fe-containing aerosols in the accumulation and coarse modes.

% Fe	Accumulation	Coarse
Minerals		
<i>Illite</i>		4.8
<i>Smectite</i>		16.4
<i>Kaolinite</i>		0.7
<i>Feldspars</i>		2.5
<i>Hematite</i>		66
Anthropogenic combustion sectors		
<i>Energy</i>	1.86	35.28
<i>Industrial</i>	1.46	27.67
<i>Residential & Commercial</i>	4.34 10 ⁻⁴	1.35 10 ⁻³
<i>Shipping</i>	0.14	0.36
<i>Waste treatment</i>	3.75	1.40
Biomass Burning	0.63	2.30

Table S2. Aqueous phase chemical mechanism and reaction rate constants. The photolysis frequencies (J) are expressed in s⁻¹, and the aqueous reactions (K) are expressed in L mol⁻¹ s⁻¹.

Aqueous-phase Reactions	J _{max} /K ₂₉₈	E _a /R	Reference
Photolysis			
J01 O ₃ + hν (+ H ₂ O) → H ₂ O ₂ + O ₂	a		
J02 H ₂ O ₂ + hν → 2 OH	a		
J03 NO ₃ + hν → NO + O ₂	a		
J04 NO ₃ + hν → NO ₂ + O ₃	a		
J05 NO ₂ ⁻ + hν (+ H ⁺) → NO + OH	a		
J06 NO ₂ ⁻ + hν (+ H ⁺) → NO ₂ + OH	a		
J07 CH ₃ O ₂ H + hν (+ O ₂) → CH ₂ (OH) ₂ + HO ₂ + OH	a		
J08 Fe ³⁺ + hν (+ H ₂ O) → Fe ²⁺ + OH + H ⁺	6.41 10 ⁻⁶ b		Deguillaume et al. (2004)
J09 [Fe(OH)] ²⁺ + hν → Fe ²⁺ + OH	5.63 10 ⁻³ b		Deguillaume et al. (2004)
J10 [Fe(OH) ₂] ⁺ + hν → Fe ²⁺ + OH + HO ⁻	7.52 10 ⁻³ b		Deguillaume et al. (2004)
J11 [Fe(SO ₄)] ⁺ + hν (+ H ₂ O) → Fe ²⁺ + SO ₄ ²⁻ + OH + H ⁺	4.51 10 ⁻⁵ b		Deguillaume et al. (2004)
J12 [Fe(OXL) ₂] ⁻ + hν (+ O ₂) → Fe ²⁺ + OXL ²⁻ + O ₂ + 2 CO ₂	2.47 10 ⁻² b		Ervens et al. (2003)
H₂O₂ chemistry			
K001 O ₃ + OH → HO ₂ + O ₂	1.1 10 ⁸		Deguillaume et al. (2010)
K002 O ₃ + HO ₂ → OH + 2 O ₂	1.0 10 ⁴		Deguillaume et al. (2010)
K003 O ₃ + O ₂ ⁻ (+ H ₂ O) → OH + O ₂ + HO ⁻	1.5 10 ⁹	2200	Deguillaume et al. (2010)
K004 HO ₂ + OH → O ₂ + H ₂ O	1.0 10 ¹⁰		Ervens et al. (2003)
K005 O ₂ ⁻ + OH → O ₂ + HO ⁻	1.1 10 ¹⁰	2120	Ervens et al. (2003)
K006 HO ₂ + HO ₂ → H ₂ O ₂ + O ₂	8.3 10 ⁵	2720	Ervens et al. (2003)
K007 HO ₂ + O ₂ ⁻ (+ H ⁺) → H ₂ O ₂ + O ₂	9.7 10 ⁷	1060	Ervens et al. (2003)
K008 OH + OH → H ₂ O ₂	3.6 10 ⁹	930	Deguillaume et al. (2010)
K009 H ₂ O ₂ + OH → HO ₂ + H ₂ O	3.0 10 ⁷	1680	Ervens et al. (2003)
Nitrogen chemistry			
K010 NO + OH → NO ₂ ⁻ + H ⁺	2.2 10 ¹⁰	1500	Deguillaume et al. (2010)
K011 NO ₂ + NO (+ H ₂ O) → 2 NO ⁻ + 2 H ⁺	3.0 10 ⁸		Deguillaume et al. (2010)
K012 NO ₂ + NO ₂ (+ H ₂ O) → HONO + NO ₃ ⁻ + H ⁺	8.4 10 ⁷	-2900	Ervens et al. (2003)
K013 NO ₂ + OH → NO ₃ ⁻ + H ⁺	1.2 10 ¹⁰		Ervens et al. (2003)
K014 NO ₃ + HO ₂ → NO ₃ ⁻ + O ₂ + H ⁺	3.0 10 ⁹		Ervens et al. (2003)
K015 NO ₃ + O ₂ ⁻ → NO ₃ ⁻ + O ₂	3.0 10 ⁹		Ervens et al. (2003)
K016 NO ₃ + H ₂ O ₂ → NO ₃ ⁻ + HO ₂ + H ⁺	4.9 10 ⁶	2000	Deguillaume et al. (2004)
K017 NO ₃ + HO ⁻ → NO ₃ ⁻ + OH	9.4 10 ⁷	2700	Ervens et al. (2003)
K018 NO ₂ ⁻ + O ₃ → NO ₃ ⁻ + O ₂	5.0 10 ⁵	7000	Ervens et al. (2003)
K019 HONO + OH → NO ₂ + H ₂ O	1.0 10 ¹⁰		Deguillaume et al. (2010)
K020 NO ₂ ⁻ + OH → NO ₂ + HO ⁻	1.1 10 ¹⁰		Ervens et al. (2003)
K021 NO ₂ ⁻ + CO ₃ ²⁻ → NO ₂ + CO ₃ ²⁻	6.6 10 ⁵	850	Ervens et al. (2003)
Sulfur chemistry			
K022 SO ₂ + O ₃ (+ H ₂ O) → HSO ₄ ⁻ + O ₂ + H ⁺	2.4 10 ⁴		Seinfeld and Pandis (2006)
K023 HSO ₃ ⁻ + O ₃ → HSO ₄ ⁻ + O ₂	3.7 10 ⁵	5530	Seinfeld and Pandis (2006)
K024 SO ₃ ²⁻ + O ₃ → SO ₄ ²⁻ + O ₂	1.5 10 ⁹	5280	Seinfeld and Pandis (2006)
K025 HSO ₃ ⁻ + H ₂ O ₂ (+ H ⁺) → H ₂ SO ₄ + H ₂ O	s		Seinfeld and Pandis (2006)
K026 SO ₂ + HO ₂ (+ H ₂ O) → H ₂ SO ₄ + OH	1.0 10 ⁶		Seinfeld and Pandis (2006)
K027 SO ₂ + O ₂ ⁻ (+ H ₂ O) → HSO ₃ ⁻ + OH + HO ⁻	1.0 10 ⁵		Seinfeld and Pandis (2006)
K028 HSO ₃ ⁻ + CH ₃ O ₂ H (+ H ⁺) → SO ₃ ²⁻ + CH ₃ OH + 2H ⁺	1.7 10 ⁷	3160	Seinfeld and Pandis (2006)
Carbonate chemistry			
K029 HCO ₃ ⁻ + OH → CO ₃ ²⁻ + H ₂ O	1.7 10 ⁷	1900	Ervens et al. (2003)
K030 CO ₃ ²⁻ + OH → CO ₃ ²⁻ + HO ⁻	3.9 10 ⁸	2840	Ervens et al. (2003)
K031 HCO ₃ ⁻ + NO ₃ → CO ₃ ²⁻ + NO ₃ ⁻ + H ⁺	4.1 10 ⁷		Ervens et al. (2003)
K032 CO ₃ ²⁻ + NO ₃ → CO ₃ ²⁻ + NO ₃ ⁻	4.1 10 ⁷		Ervens et al. (2003)
K033 CO ₃ ²⁻ + O ₃ → CO ₂ + O ₂ ⁻ + O ₂	1.0 10 ⁵		Ervens et al. (2003)
K034 CO ₃ ²⁻ + HO ₂ → HCO ₃ ⁻ + O ₂	6.5 10 ⁸		Ervens et al. (2003)
K035 CO ₃ ²⁻ + O ₂ ⁻ → CO ₃ ²⁻ + O ₂	6.5 10 ⁸		Ervens et al. (2003)
K036 CO ₃ ²⁻ + H ₂ O ₂ → HCO ₃ ⁻ + HO ₂	4.3 10 ⁵		Ervens et al. (2003)
K037 CO ₃ ²⁻ + NO ₂ → CO ₂ + NO ₃ ⁻	1.0 10 ⁹		Ervens et al. (2003)
K038 CO ₃ ²⁻ + CO ₃ ²⁻ (+ O ₂) → 2 O ₂ ⁻ + 2 CO ₂	2.2 10 ⁶		Ervens et al. (2003)
Organic chemistry			
K039 CH ₃ O ₂ H + OH → 0.8 (CH ₃ O ₂ + H ₂ O) + 0.2 (HCOOH + HO ₂)	3.0 10 ⁷	1680	Ervens et al. (2003)
K040 CH ₃ O ₂ H + CO ₃ ²⁻ → CH ₃ O ₂ ⁻ + HCO ₃ ⁻	4.3 10 ⁵		Ervens et al. (2003)

Table S3: Henry's law solubility constants (H), mass accommodation coefficients (α) and gas phase diffusion coefficients (D_g) used in aqueous-phase chemistry scheme.

Trace gas	H (mol m ⁻³ Pa ⁻¹)	-ΔH R ⁻¹ (K)	Reference	α	Reference	D _g (m ² s ⁻¹)	Reference
O ₃	1.0 10 ⁻⁴	2800	1	0.05	2	1.48 10 ⁻⁵	2
H ₂ O ₂	9.1 10 ²	6600	1	0.11	2	1.46 10 ⁻⁵	2
HO ₂	6.8		1	0.01	2	1.04 10 ⁻⁵	2
OH	3.8 10 ⁻¹		1	0.05	2	1.53 10 ⁻⁵	2
NO	1.9 10 ⁻⁵	1600	1	as for NO ₂	2	as for NO ₂	
NO ₂	9.9 10 ⁻⁵		1	0.0015	2	1.92 10 ⁻⁵	2
NO ₃	3.8 10 ⁻⁴		1	0.004	2	1.00 10 ⁻⁵	2
HONO	4.8 10 ⁻¹	4800	1	0.5	2	1.30 10 ⁻⁵	2
HNO ₃	8.8 10 ²		1	0.054	2	1.32 10 ⁻⁵	2
SO ₂	1.3 10 ⁻²	2900	1	0.035	2	1.28 10 ⁻⁵	2
CO ₂	3.3 10 ⁻⁴	2400	1	0.0002	2	1.55 10 ⁻⁵	2
CH ₃ O ₂	1.5 10 ⁻¹	3700	1	as for CH ₃ O ₂ H	2	as for CH ₃ O ₂ H	2
CH ₃ O ₂ H	2.9	5200	1	0.0038	2	1.31 10 ⁻⁵	2
HCHO	3.2 10 ⁻¹	6800	1	0.02	2	1.64 10 ⁻⁵	2
CH ₃ OH	2.0	5600	1	0.015	2	1.16 10 ⁻⁵	2
HCOOH	8.8 10 ¹	6100	1	0.012	2	1.53 10 ⁻⁵	2
GLYAL	4.1 10 ²	4600	1	as for GLY		as for GLY	
GLY	4.1 10 ³	7500	1	0.023	3	1.15 10 ⁻⁵	3
MGLY	3.4 10 ¹	7500	1	as for GLY		as for GLY	
HYAC	7.7 10 ¹		1	0.0176	4	9.50 10 ⁻⁷	4
CH ₃ CHO	1.3 10 ⁻¹	5900	1	0.03	2	1.22 10 ⁻⁵	2
CH ₃ CH ₂ OH	1.9	6400	1	0.0082	2	9.50 10 ⁻⁶	2
CH ₃ COOH	4.0 10 ¹	6200	1	0.019	3	1.24 10 ⁻⁵	2
PRV	3.1 10 ³	5100	1	as for CH ₃ COOH		as for CH ₃ COOH	
GLX	1.1 10 ²	4800	1	as for CH ₃ COOH		as for CH ₃ COOH	
H ₂ OXL	3.1 10 ⁴	7300	1	as for CH ₃ COOH		as for CH ₃ COOH	

1) Sander (2015) and references therein.

2) Herrmann et al. (2000) and references therein.

3) Lim et al. (2005) and references therein.

4) Ervens et al. (2003) and references therein.

Table S4. Dissolution scheme for iron-containing combustion and mineral dust aerosols.

Iron pool	Scheme ^a	K ₂₉₈ ^a	m ^b	K _{eq} ^c	n ^d	Reference	
D01	Combustion Fe ^e	H ⁺	5.24 10 ⁻⁸	0.36		Ito (2015)	
D02		OXL	3.85 10 ⁻⁶	1		Ito (2015)	
D03		hν ^f	4.10 10 ⁻⁶	1		Ito (2015)	
D04	Ferrihydrite	H ⁺	7.13 10 ⁻⁵	1.1	1550	3	Ito and Shi (2016)
D05		OXL	4.61 10 ⁻⁸	0.069	1550	3	Ito and Shi (2016)
D06		hν ^f	4.61 10 ⁻⁸	0.069			Ito and Shi (2016)
D07	Nano-Fe oxides	H ⁺	1.43 10 ⁻⁴	1.6	42	2.75	Ito and Shi (2016)
D08		OXL	1.28 10 ⁻⁸	0.069	1550	3	Ito and Shi (2016)
D09		hν ^f	1.28 10 ⁻⁸	0.069			Ito and Shi (2016)
D10	Aluminosilicates	H ⁺	5.85 10 ⁻⁸	0.76	3.3	2.85	Ito and Shi (2016)
D11		OXL	1.68 10 ⁻⁹	0.056	1500	3	Ito and Shi (2016)
D12		hν ^f	1.68 10 ⁻⁹	0.056			Ito and Shi (2016)

^{a)} The dissolution rate constants (K) for combustion and mineral dust aerosols are expressed in mol Fe g⁻¹ s⁻¹ and defined as:

$$K = K_{228} \cdot \exp[E_{pH} \cdot (1/298 - 1/T)]$$

where, E_{pH} = -1.56 10³ · pH + 1.08 10⁴ (Bibi et al., 2014; Ito and Shi, 2016)

^{b)} m is the reaction order (Ito, 2015; Ito and Shi, 2016)

^{c)} K_{eq} is the equilibrium constant (mol² kg⁻²) (Bonneville et al., 2004; Ito and Shi, 2016)

^{d)} n is the stoichiometric ratio (Bonneville et al., 2004; Ito and Shi, 2016).

^{e)} The unit for combustion aerosol is converted from moles m⁻² s⁻¹ to mol Fe g⁻¹ s⁻¹ (Ito, 2015)

^{f)} Photoinduced dissolution rate constants are scaled on the model's H₂O₂ gas-phase photolysis frequencies.

^{g)} For the proton-promoted dissolution, suppressions are taken into account when the solution becomes supersaturated with respect to Fe(III), but any suppression due to OXL is neglected (i.e., 0 ≤ f_i ≤ 1 and g_i = 1). For oxalate-promoted dissolution, the formation of amorphous Fe(OH)₃(s) (Shi et al., 2009, 2015) is assumed to inhibit the adsorption of OXL and, thus, the Fe release from the minerals' surface (i.e., 0 ≤ f_i ≤ 1 and 0 ≤ g_i ≤ 1). For combustion aerosols, both the OXL-promoted and photo-induced dissolution rates are also considered to be suppressed by the formation of amorphous Fe(OH)₃(s) (Ito, 2015).

Table S5: Aqueous phase equilibrium constants (E_k) used in aqueous-phase chemistry scheme.

Equilibrium Reaction			E_{k298} (mol L ⁻¹)	$-\Delta H R^{-1}$ (K)	Reference
H ₂ O	↔	HO ⁻ + H ⁺	1.0 10 ⁻¹⁴	-6710	1
H ₂ O ₂	↔	HO ₂ ⁻ + H ⁺	2.2 10 ⁻¹²	-3730	1
HO ₂	↔	O ₂ ⁻ + H ⁺	3.5 10 ⁻⁵		1
CO ₂ (+ H ₂ O)	↔	H ₂ CO ₃	7.7 10 ⁻⁷	-750	2
H ₂ CO ₃	↔	HCO ₃ ⁻ + H ⁺	2.0 10 ⁻⁴		2
HCO ₃ ⁻	↔	CO ₃ ²⁻ + H ⁺	4.69 10 ⁻¹¹	-1820	2
NH ₄ OH	↔	NH ₄ ⁺ + HO ⁻	1.7 10 ⁻⁵	-450	1
SO ₂ ·H ₂ O	↔	HSO ₃ ⁻ + H ⁺	1.3 10 ⁻²	1960	1
HSO ₃ ⁻	↔	SO ₃ ²⁻ + H ⁺	6.6 10 ⁻⁸	1500	1
HONO	↔	NO ₂ ⁻ + H ⁺	5.1 10 ⁻⁴	-1260	1
HNO ₃	↔	NO ₃ ⁻ + H ⁺	15.4	8700	1
HCOOH	↔	HCOO ⁻ + H ⁺	1.77 10 ⁻⁴	-12	3
CH ₃ COOH	↔	CH ₃ COO ⁻ + H ⁺	1.75 10 ⁻⁵	-46	3
PRV	↔	PRV ⁻ + H ⁺	3.2 10 ⁻³		4
GLX	↔	GLX ⁻ + H ⁺	3.47 10 ⁻⁴	-267	4
H ₂ OXL	↔	HOXL ⁻ + H ⁺	5.6 10 ⁻²	-453	4
HOXL ⁻	↔	OXL ⁻ + H ⁺	5.42 10 ⁻⁵	-805	4
Fe ³⁺ (+ H ₂ O)	↔	[Fe(OH)] ²⁺ + H ⁺	1.1 10 ⁻⁴		3
[Fe(OH)] ²⁺ (+ H ₂ O)	↔	[Fe(OH) ₂] ⁺ + H ⁺	1.4 10 ⁻⁷		3

¹⁾ Seinfeld and Pandis (2006) and references therein.

²⁾ Herrmann et al. (2000) and references therein.

³⁾ Ervens et al. (2003) and references therein.

⁴⁾ Lim et al. (2005) and references therein.

Supplementary Equations

Mathematical formulas for correlation coefficient (R ; Eq. S1), normalized mean bias (nMB; Eq. S2), and the normalized root mean square error (nRMSE; Eq. S3), used for the statistical analysis of model comparison against observations; O_i and P_i stand for observations and predictions, respectively. N is the number of pairs (observations, predictions) that are compared.

$$R = \left[\frac{\frac{1}{N} \sum_{i=1}^N (O_i - \bar{O})(P_i - \bar{P})}{\sigma_O \sigma_P} \right] \quad (\text{Eq. S1})$$

$$NMB = \frac{\sum_{i=1}^N (M_i - O_i)}{\sum_{i=1}^N O_i} \times 100 \quad (\text{Eq. S2})$$

$$nRMSE = \frac{\sqrt{\frac{1}{N} \sum_{i=1}^N (P_i - O_i)^2}}{\sum_{i=1}^N O_i} \quad (\text{Eq. S3})$$

Supplementary Figures

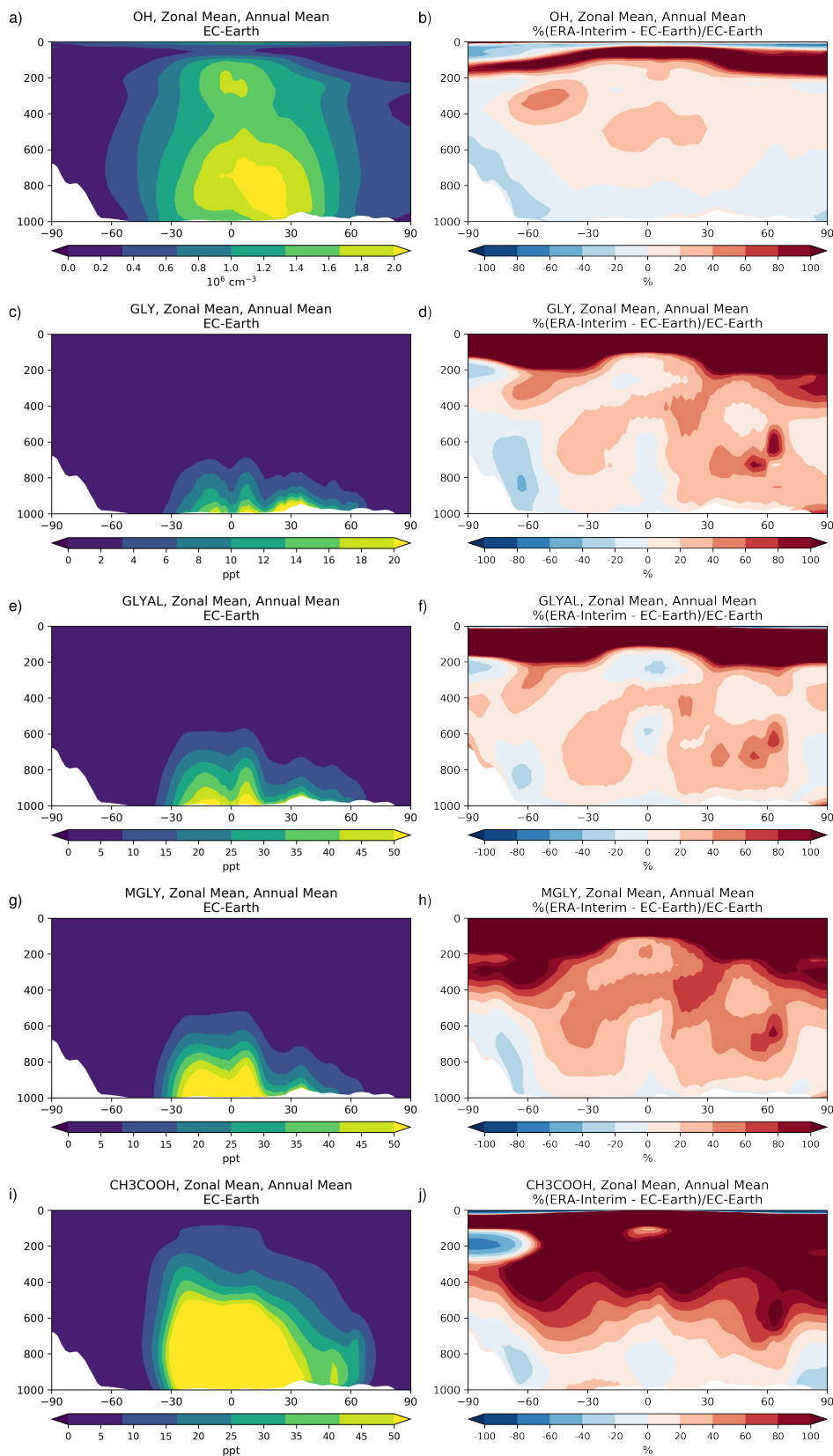


Figure S1: Annual mean zonal mean concentrations of a) OH radicals ($10^6 \text{ molec. cm}^{-3}$), c) glyoxal (ppt), e) glycolaldehyde (ppt), g) methylglyoxal (ppt), and i) acetic acid (ppt), as simulated for the EC-Earth simulation, averaged for the period 2000-2014, and the absolute differences to the ERA-Interim simulation (b,d,f,h,j).

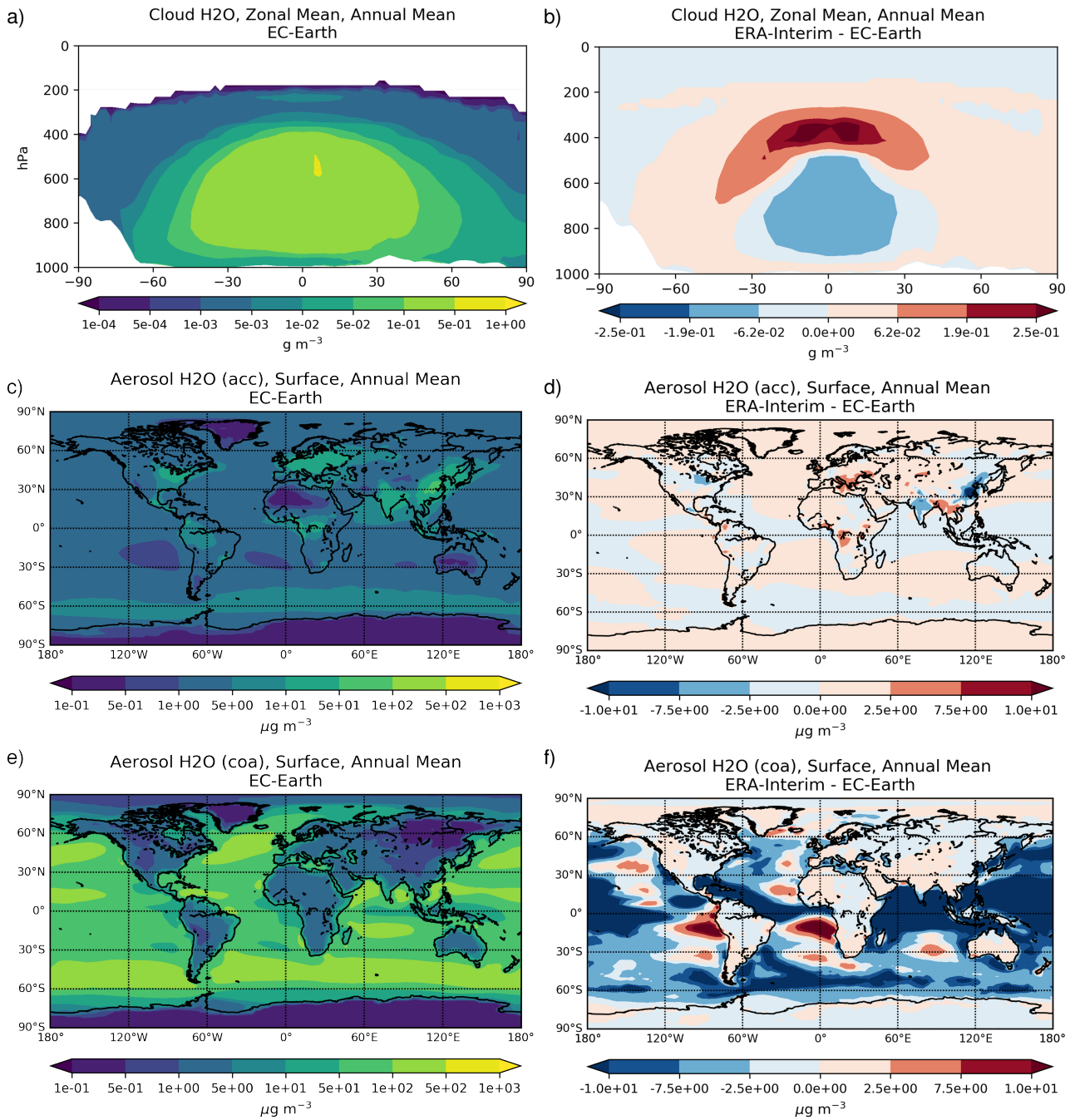


Figure S2: Annual mean of a) zonal mean concentrations of cloud water (g m^{-3}), c) surface concentrations of aerosol water associated with accumulation aerosols ($\mu\text{g m}^{-3}$), and e) surface concentrations of aerosol water associated with coarse aerosols ($\mu\text{g m}^{-3}$), as simulated for the EC-Earth simulation, averaged for the period 2000-2014, and the respective absolute differences to the ERA-Interim simulation (b,d,f).

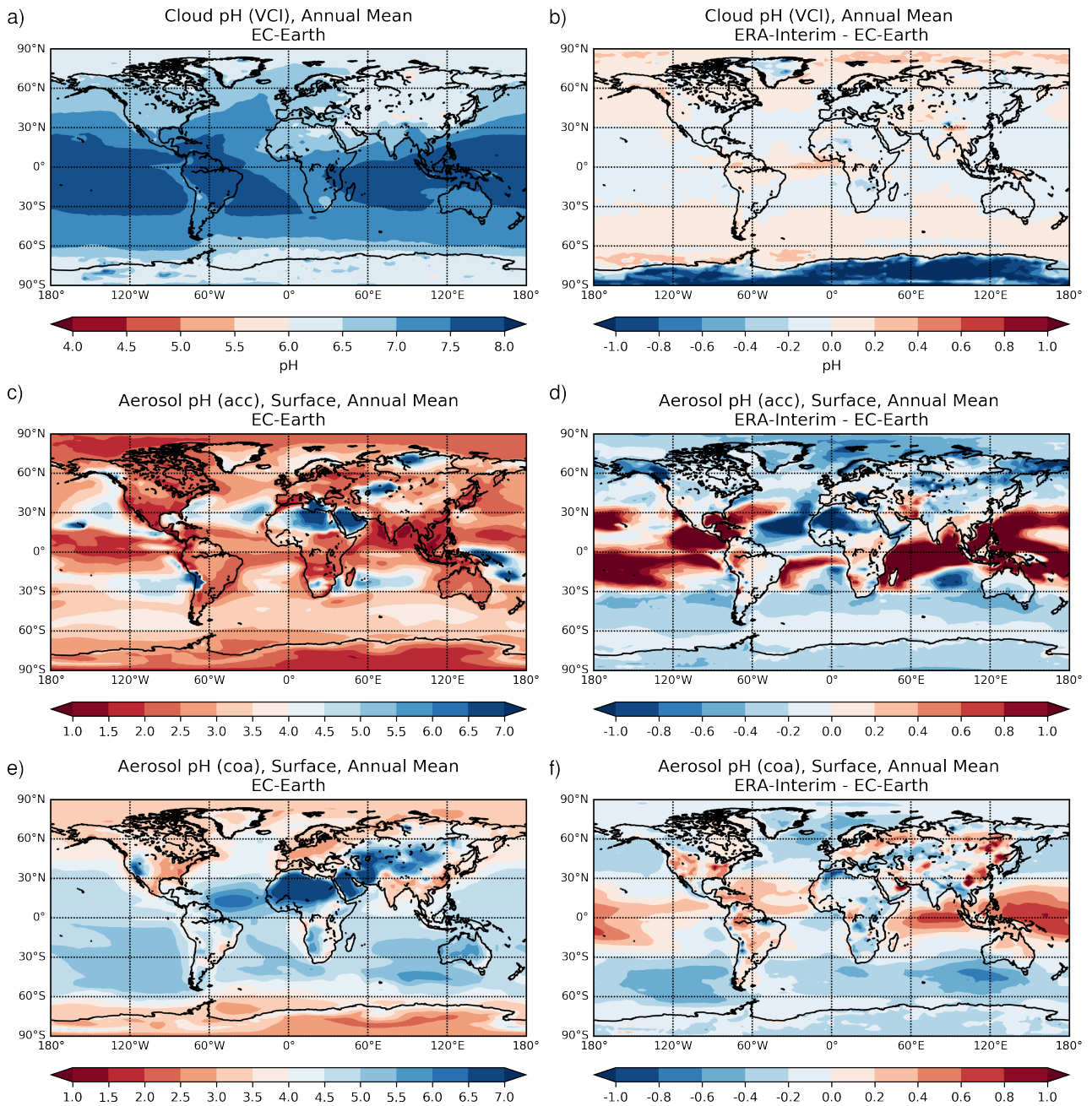


Figure S3: Annual mean a) vertical-column-integrated (VCI) liquid-water-weighted cloud water pH, c) accumulation aerosol pH at the surface, e) and coarse aerosol pH at the surface, as calculated for the EC-Earth simulation, averaged for the period 2000-2014, and the respective absolute differences to the ERA-Interim simulation (b,d,f).

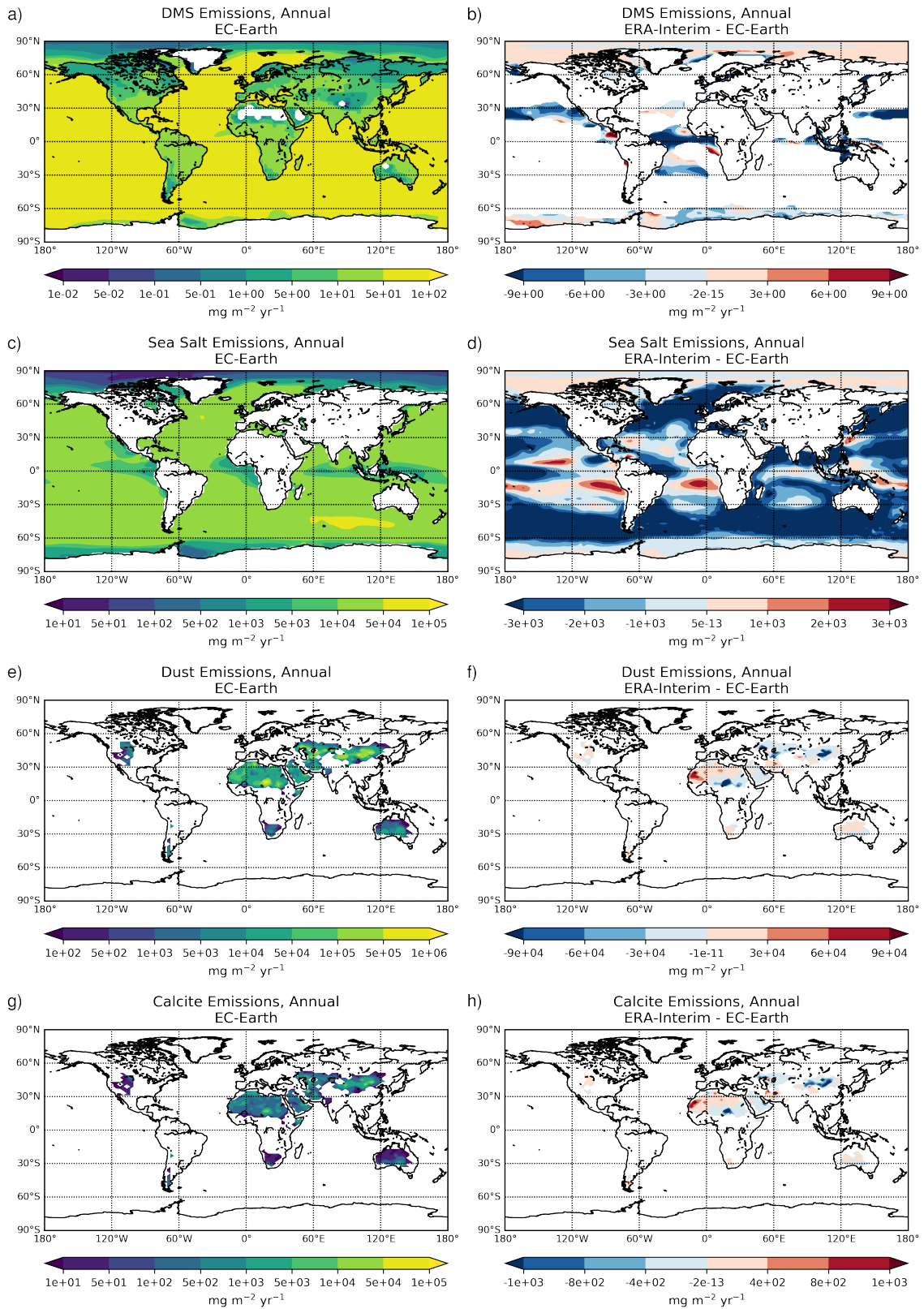


Figure S4: Annual mean emission fluxes ($\text{mg m}^{-2} \text{yr}^{-1}$) of a) DMS, c) sea salt, e) mineral dust, and g) calcite (in $\text{mg Ca m}^{-2} \text{yr}^{-1}$), as calculated for the EC-Earth simulation, averaged for the period 2000-2014, and the respective absolute differences to the ERA-Interim simulation (b,d,f,h).

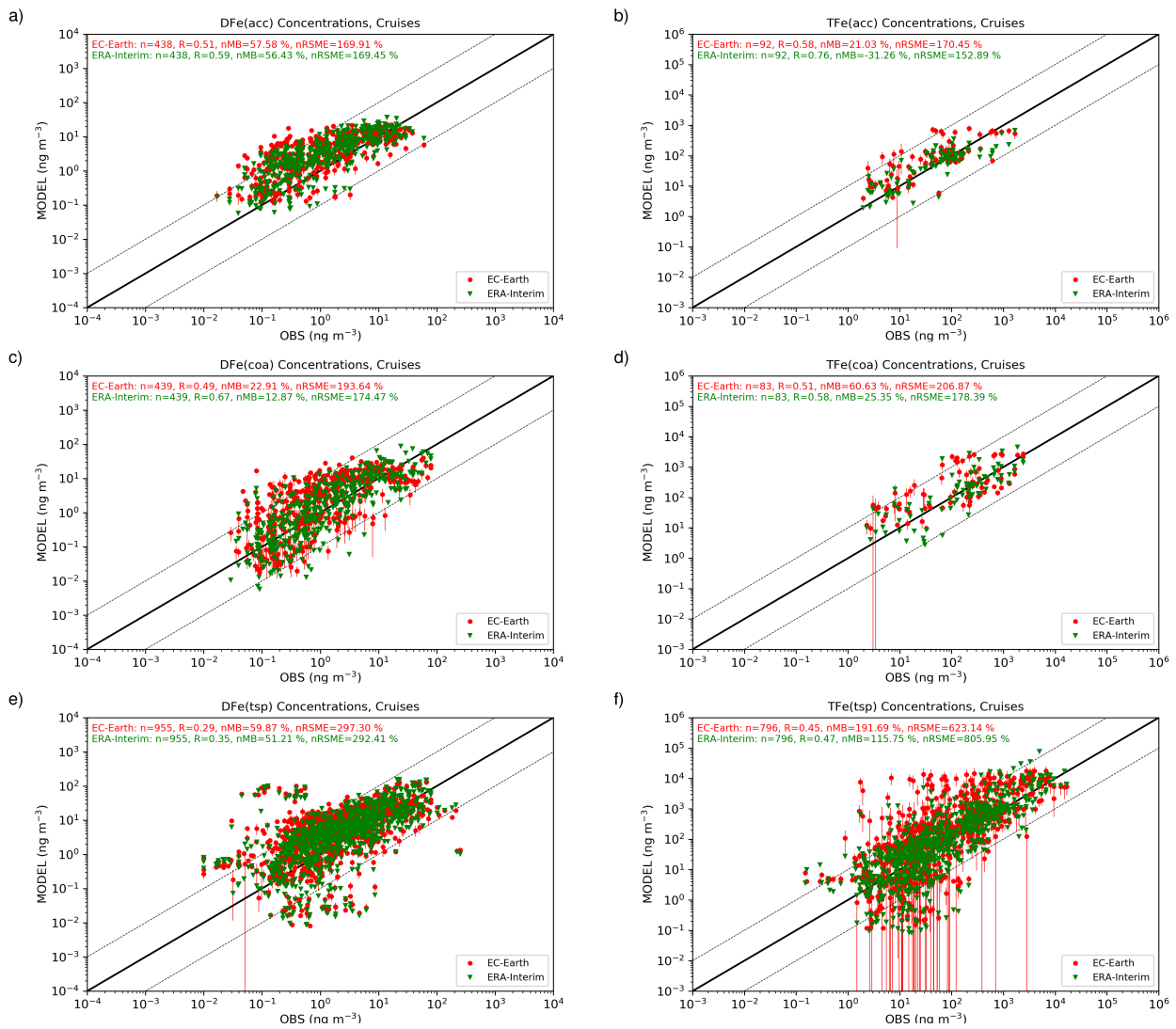


Figure S5: Scatterplot comparisons of cruise observations (see text) for accumulation (top), coarse (middle) and total suspended matter (bottom) of dissolved iron (DFe; a,c,e) and total iron (TFe; b,d,f) aerosols (ng m^{-3}) with EC-Earth (red circles) and ERA-Interim (green triangles) simulations; the solid line represents the 1 : 1 correspondence and the dashed lines show the 10 : 1 and 1 : 10 relationships, respectively and for the EC-Earth simulation the error bars represent the standard error of the multi-annual mean for the individual observational period. Summary statistics for all points are also included (color coded).

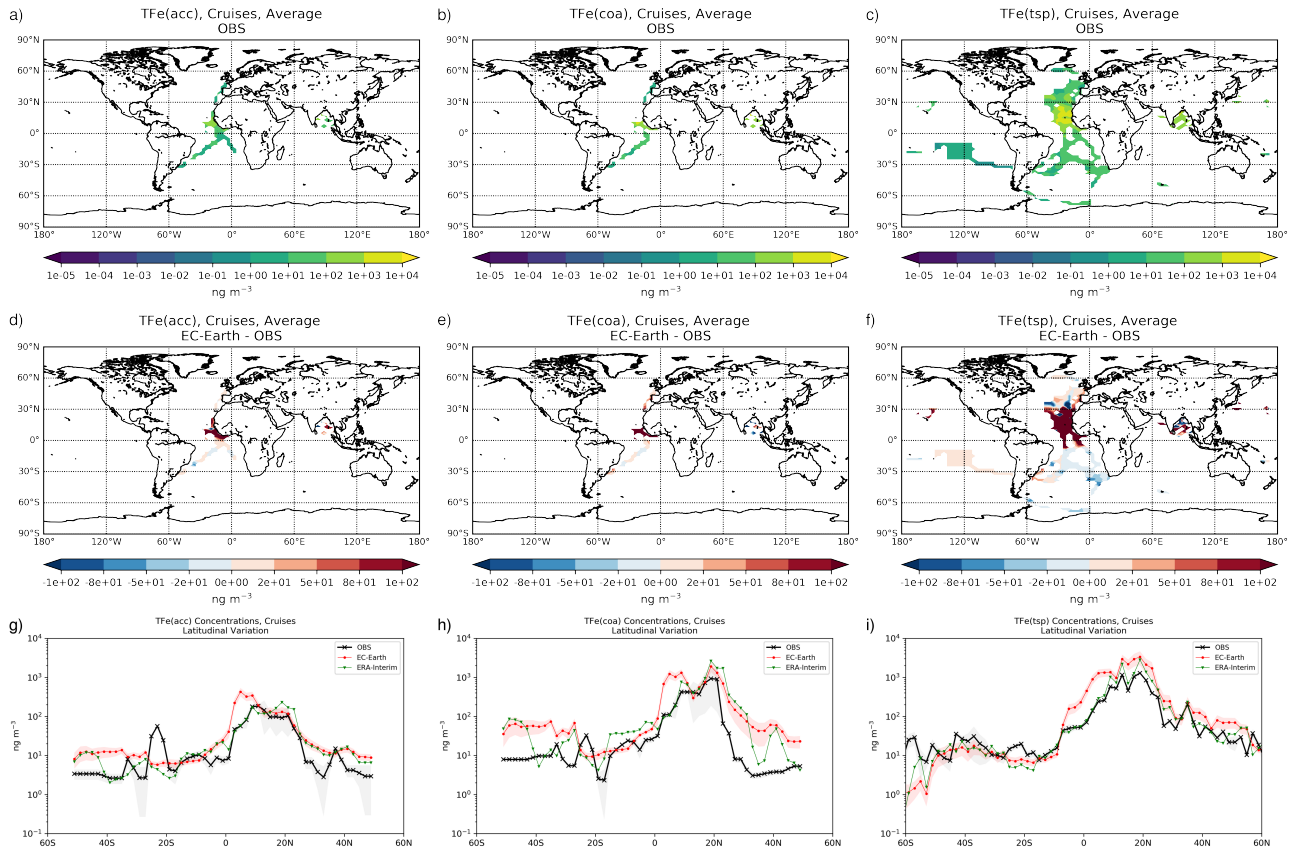


Figure S6: Observed total iron (TFe) concentrations (ng m^{-3}) of a) accumulation aerosols, b) coarse aerosols, and c) total suspended particles (tsp), the respective absolute differences to the ERA-Interim simulation (d, e, f), and the comparison to observations (black X-line) in latitudinal order (g,e,f) with the EC-Earth (red circle-line) and ERA-Interim (green triangle-line) simulations; the grey shaded areas correspond to the standard deviation of the observations and the red shaded areas correspond to the standard error of the multi-annual mean for the individual observational period for the EC-Earth simulations.

References

- Bibi, I., Singh, B. and Silvester, E.: Dissolution kinetics of soil clays in sulfuric acid solutions: Ionic strength and temperature effects, *Appl. Geochemistry*, 51, 170–183, doi:10.1016/j.apgeochem.2014.10.004, 2014.
- Bonneville, S., Van Cappellen, P. and Behrends, T.: Microbial reduction of iron(III) oxyhydroxides: effects of mineral solubility and availability, *Chem. Geol.*, 212(3), 255–268, doi:10.1016/j.chemgeo.2004.08.015, 2004.
- Carlton, A. G., Turpin, B. J., Altieri, K. E., Seitzinger, S., Reff, A., Lim, H.-J. and Ervens, B.: Atmospheric oxalic acid and SOA production from glyoxal: Results of aqueous photooxidation experiments, *Atmos. Environ.*, 41(35), 7588–7602, doi:10.1016/j.atmosenv.2007.05.035, 2007.
- Chen, H. and Grassian, V. H.: Iron Dissolution of Dust Source Materials during Simulated Acidic Processing: The Effect of Sulfuric, Acetic, and Oxalic Acids, *Environ. Sci. Technol.*, 130829091001000, doi:10.1021/es401285s, 2013.
- Cornell, R. M., Schwertmann, U. and John Wiley & Sons.: *The iron oxides : structure, properties, reactions, occurrences, and uses*, Wiley-VCH., 2003.
- Deguillaume, L., Leriche, M., Monod, A. and Chaumerliac, N.: The role of transition metal ions on HO_x radicals in clouds: a numerical evaluation of its impact on multiphase chemistry, *Atmos. Chem. Phys.*, 4(1), 95–110, doi:10.5194/acp-4-95-2004, 2004.
- Deguillaume, L., Tilgner, A., Schrödner, R., Wolke, R., Chaumerliac, N. and Herrmann, H.: Towards an operational aqueous phase chemistry mechanism for regional chemistry-transport models: CAPRAM-RED and its application to the COSMO-MUSCAT model, *J. Atmos. Chem.*, 64(1), 1–35, doi:10.1007/s10874-010-9168-8, 2009.
- Deguillaume, L., Desboeufs, K. V., Leriche, M., Long, Y. and Chaumerliac, N.: Effect of iron dissolution on cloud chemistry: from laboratory measurements to model results, *Atmos. Pollut. Res.*, 1(4), 220–228, doi:10.5094/APR.2010.029, 2010.
- Ervens, B., George, C., Williams, J. E., Buxton, G. V., Salmon, G. A., Bydder, M., Wilkinson, F., Dentener, F., Mirabel, P., Wolke, R. and Herrmann, H.: CAPRAM 2.4 (MODAC mechanism): An extended and condensed tropospheric aqueous phase mechanism and its application, *J. Geophys. Res.*, 108(D14), 4426, doi:10.1029/2002JD002202, 2003.
- Ervens, B., Feingold, G., Frost, G. J. and Kreidenweis, S. M.: A modeling study of aqueous production of dicarboxylic acids: 1. Chemical pathways and speciated organic mass production, *J. Geophys. Res.*, 109(D15), D15205, doi:10.1029/2003JD004387, 2004.
- Herrmann, H., Ervens, B., Jacobi, H. W., Wolke, R., Nowacki, P. and Zellner, R.: CAPRAM2.3: A chemical aqueous phase radical mechanism for tropospheric chemistry, *J. Atmos. Chem.*, 36(3), 231–284, doi:10.1023/A:1006318622743, 2000.
- Herrmann, H., Tilgner, A., Barzagli, P., Majdik, Z., Gligorovski, S., Poulain, L. and Monod, A.: Towards a more detailed description of tropospheric aqueous phase organic chemistry: CAPRAM 3.0, *Atmos. Environ.*, 39(23–24), 4351–4363, doi:10.1016/j.atmosenv.2005.02.016, 2005.
- Ito, A.: Atmospheric Processing of Combustion Aerosols as a Source of Bioavailable Iron, *Environ. Sci. Technol. Lett.*, 2(3), 70–75, doi:10.1021/acs.estlett.5b00007, 2015.
- Ito, A. and Shi, Z.: Delivery of anthropogenic bioavailable iron from mineral dust and combustion aerosols to the ocean, *Atmos. Chem. Phys.*, 16(1), 85–99, doi:10.5194/acp-16-85-2016, 2016.
- Ito, A., Lin, G. and Penner, J. E.: Radiative forcing by light-absorbing aerosols of pyrogenetic iron oxides, *Sci. Rep.*, 8(1),

7347, doi:10.1038/s41598-018-25756-3, 2018.

Lim, H.-J., Carlton, A. G. and Turpin, B. J.: Isoprene Forms Secondary Organic Aerosol through Cloud Processing: Model Simulations, *Environ. Sci. Technol.*, 39(12), 4441–4446, doi:10.1021/es048039h, 2005.

Lin, G., Sillman, S., Penner, J. E. and Ito, A.: Global modeling of SOA: the use of different mechanisms for aqueous-phase formation, *Atmos. Chem. Phys.*, 14(11), 5451–5475, doi:10.5194/acp-14-5451-2014, 2014.

Ramos, M. E., Garcia-Palma, S., Rozalen, M., Johnston, C. T. and Huertas, F. J.: Kinetics of montmorillonite dissolution, *Chem. Geol.*, 363, 283–292, doi:10.1016/j.chemgeo.2013.11.014, 2014.

Sander, R.: Compilation of Henry's law constants (version 4.0) for water as solvent, *Atmos. Chem. Phys.*, 15(8), 4399–4981, doi:10.5194/acp-15-4399-2015, 2015.

Sedlak, D. L. and Hoigné, J.: The role of copper and oxalate in the redox cycling of iron in atmospheric waters, *Atmos. Environ. Part A, Gen. Top.*, 27(14), 2173–2185, doi:10.1016/0960-1686(93)90047-3, 1993.

Seinfeld, J. H. and Pandis, S. N.: *Atmospheric Chemistry and Physics: From Air Pollution to Climate Change.*, 2006.

Shi, Z., Krom, M. D., Bonneville, S., Baker, A. R., Jickells, T. D. and Benning, L. G.: Formation of Iron Nanoparticles and Increase in Iron Reactivity in Mineral Dust during Simulated Cloud Processing, *Environ. Sci. Technol.*, 43(17), 6592–6596, doi:10.1021/es901294g, 2009.

Shi, Z., Krom, M. D., Bonneville, S. and Benning, L. G.: Atmospheric Processing Outside Clouds Increases Soluble Iron in Mineral Dust, *Environ. Sci. Technol.*, 49(3), 1472–1477, doi:10.1021/es504623x, 2015.

Siffert, C. and Sulzberger, B.: Light-Induced Dissolution of Hematite in the Presence of Oxalate: A Case Study, *Langmuir*, 7(8), 1627–1634, doi:10.1021/la00056a014, 1991.

Tan, Y., Lim, Y. B., Altieri, K. E., Seitzinger, S. P. and Turpin, B. J.: Mechanisms leading to oligomers and SOA through aqueous photooxidation: insights from OH radical oxidation of acetic acid and methylglyoxal, *Atmos. Chem. Phys.*, 12(2), 801–813, doi:10.5194/acp-12-801-2012, 2012.